International Journal of Multiphase Flow 95 (2017) 135–143

Contents lists available at ScienceDirect

International Journal of Multiphase Flow

journal homepage: www.elsevier.com/locate/ijmulflow

Effect of insoluble surfactant on turbulent bubbly flows in vertical channels

Jiacai Lu[a,*], Metin Muradoglu[b], Gretar Tryggvason[a]

[a] Department of Aerospace and Mechanical Engineering, University of Notre Dame, Notre Dame, IN, USA
[b] Department of Mechanical Engineering, Koc University, Istanbul, Turkey

ARTICLE INFO

Article history:
Received 9 November 2016
Revised 2 May 2017
Accepted 19 May 2017
Available online 30 May 2017

Keywords:
Bubbly flow
Turbulence
Insoluble surfactant
Flow structure

ABSTRACT

The effect of an insoluble surfactant on the structure of turbulent bubbly upflow in a vertical channel is examined by direct numerical simulations (DNS). For nearly spherical bubbles the presence of a surfactant reduces the lateral lift on the bubbles and changes the structure of the flow in major ways. Clean bubbles are driven to the walls by the lift force and the void fraction distribution has a well defined peak near the walls, resulting in significant reduction in flow rate. Bubbles with strong enough surfactants do not experience significant lateral lift and remain in the bulk flow. Indeed, when surfactant is present the addition of bubbles to a turbulent flow has relatively little effect on the flow, once the pressure gradient is adjusted to account for the reduced weight of the mixture.

1. Introduction

Direct numerical simulations, or DNS, can now produce data for turbulent bubbly flows of sufficient complexity that the results should have direct relevance to experiments and practical situations. Direct comparisons do, however, remain problematic for a number of reasons. Not only is the Reynolds number for most experiments considerably higher than is achievable in DNS but experimental results often lack the detailed information necessary to fully specify the flow, such as the size distribution of bubbles. Of even greater concern is that real bubbly flows almost always contain surfactants (or contaminants) that can result in uneven surface tension over a bubble surface and except for experiments specifically designed to examine the effect of surfactants, most experimental results do not include any quantification of the presence of surfactants. It is well known that surfactants reduce the rise velocity of nearly spherical and moderately deformed bubbles, but much less is known about the effect of surfactants on the lift force on bubbles. The lift force is critical in determining the void fraction distribution in a channel or a pipe with many bubbles, and recent experimental studies have shown that surfactants affect the distribution in a very significant way (So et al., 2002; Takagi et al., 2008). Here we examine the effect of insoluble surfactant on the collective motion of several bubbles in a turbulent upflow in a vertical channel.

For nearly spherical bubbles in laminar flow in vertical channels, Lu et al. (2006) showed that the void fraction distribution is dominated by the lift on the bubbles and results in a bubble rich wall layer for upflow and a bubble free wall layer for downflow. The transfer of bubbles toward the wall for upflow increased the weight of the mixture in the core of the channel and the transfer away from the wall for downflow decreases the mixture weight. In both cases the transfer of bubbles continues until the weight of the mixture in the core balances the imposed pressure gradient (assuming enough bubbles). Lu et al. (2006) showed that this observation leads to a very simple expression for the void fraction distribution and allowed the flow rate to be determined analytically for downflow. For upflow the formation of a wall layer takes place quickly but then the presence of the wall layer reduces the flow rate significantly, for a given pressure gradient. A similar setup, but for turbulent flow and a larger number of bubbles, was examined by Lu and Tryggvason (2008) who found that the void fraction was well predicted by the model of Lu et al. (2006), that the flow rate was significantly reduced once the wall-layer formed, and that the bubbles in the wall layer formed horizontal clusters.

Although wall peaked void fraction profiles are often observed experimentally for bubbly upflow in vertical channels (Serizawa et al., 1975, for example), the distribution is generally not as sharp as seen in the DNS simulations, even for small bubbles. The only experimental study that has showed similar wall layers is So et al. (2002) who examined effect of adding a small amount of surfactant to bubbly upflow, where the size of the injected

* Corresponding author.
E-mail address: jlu2@nd.edu (J. Lu).

http://dx.doi.org/10.1016/j.ijmultiphaseflow.2017.05.003
0301-9322/

bubbles was tightly controlled to keep the size distribution small. The addition of just a small amount prevented coalescence, but apparently had essentially no other effect. Indeed, Ogasawara et al. (2009) showed later that adding more surfactant eliminated the wall layers. The experiments by So et al. (2002) also showed that the velocity profile became more blunted and that the turbulence intensity in the channel core was reduced. As pointed out in Lu and Tryggvason (2008) the similarity between their results and the experimental results strongly suggest that the bubbles in So et al. (2002) are, for all practical purpose "clean," and that it is the absence of coalescence that is responsible for the wall layers and the change in flow structure. The effect of the wall layers on the flow rate or the pressure drop was not examined by So et al. (2002) or Ogasawara et al. (2009).

DNS have also been used to examine the collective motion of deformable bubbles, where the lift force is generally nearly zero and sometimes slightly negative so the bubbles do not form wall layers and remain distributed throughout the channel (Dabiri et al., 2013; Ling et al., 2017). Compared to a single-phase flow with the same effective pressure gradient (pressure gradient adjusted for the weight of the mixture), the average velocity profile for deformable bubbles and thus the flow rate are nearly the same. As the deformability of the bubbles is reduced, the flow changes rather abruptly from one state to the other, see Lu and Tryggvason (2008) and Dabiri et al. (2013). For other DNS studies of the collective behavior of clean bubbles see, for example, Bunner and Tryggvason (2003), van Sint Annaland et al. (2006), Bolotnov et al. (2011, 2008), Bolotnov (2013), Tanaka (2011), Dijkhuizen et al. (2010a, 2010b), Balcázar et al. (2015) and Bois and du Cluzeau (2017). Several authors have also examined the collective motion of non-deformable particles. We will not review those studies, but mention Santarelli and Fröhlich (2015); 2016), who examined the collective motion of several hundred buoyant particles. Their results did not show the strong lateral motion seen for clean bubbles, since their results are likely to be similar to what we see for "fully" contaminated bubbles where the effects of the surfactant are sufficiently strong to completely immobilize the bubble surface.

A large number of investigators have experimentally examined the effect of surfactants on the rise of bubbles and it is now well established that surfactants generally reduce the rise velocity of small bubbles, but for larger bubbles, where the effect of surface tension is small, the reduction is insignificant (see Clift et al., 1978; Takagi and Matsumoto, 2011, for example). We will not review those studies here but refer the reader to Takagi and Matsumoto (2011).

In numerical simulations of the effect of surfactants on the bubbles have, in most cases, been assumed to be spherical, such as in the work of Fukuta et al. (2005); 2008) who examined the lift on bubbles in a linear shear flow. A few authors have, however, examined deformable ones. Jan (1994) examined the rise of axisymmetric deformable bubbles with insoluble surfactant and Muradoglu and Tryggvason (2008) considered the effect of soluble surfactants on two-dimensional bubbles. Simulations of single deformable three-dimensional bubbles are described in Muradoglu and Tryggvason (2014) for soluble surfactants and in de Jesus et al. (2015) for insoluble ones. Muradoglu and Tryggvason (2014) did, in particular, examine the motion of a single bubble near a wall in upflow and showed that while a nearly spherical bubble is pushed to the wall, a bubble in a sufficiently strong surfactant solution drifts away from the wall. Although the deformation of a drop in a shear flow was examined in de Jesus et al. (2015), buoyancy was not included so the drop was stationary.

Here we examine the effect of insoluble surfactant on the collective motion of nearly spherical bubbles in turbulent upflow, using DNS. The goal of the study is to show that the reduction in flow rate when clean non-coalescing bubbles form wall layers is largely eliminated by the addition of surfactants, as well as to examine the changes in the void fraction distribution and flow structure.

2. Numerical method and computational setup

The computational domain is rectangular, bounded by two vertical walls and with periodic boundary conditions in the spanwise and streamwise directions. The flow is described by the Navier-Stokes equations, written for the whole domain,

$$\rho\frac{\partial \mathbf{u}}{\partial t}+\rho\nabla\mathbf{u}\mathbf{u}=-\nabla p'-\beta_o\mathbf{k}+(\rho-\rho_{av})\mathbf{g}+\nabla\cdot\mu(\nabla\mathbf{u}+\nabla\mathbf{u}^T)+\int_F\nabla_f\cdot\left(\sigma\mathbf{t}_f\right)\delta\left(\mathbf{x}-\mathbf{x}_f\right)dA_f, \quad (1)$$

Here, $\mathbf{u}$ is the velocity vector, ρ and μ are the discontinuous density and viscosity fields, respectively, $\mathbf{g}=-g\mathbf{k}$ is the gravity acceleration, ρ_{av} is the average density of the mixture and $\beta_o=(dp_0/dz)+\rho_{av}g$. σ is the surface tension and δ is a three-dimensional delta function constructed by repeated multiplication of one-dimensional delta functions. $\mathbf{t}_f$ is the unit tangent vector on the front, $\mathbf{x}$ is the point at which the equation is evaluated, and $\mathbf{x}_f$ is the position of the front. The flow is driven upward by an imposed pressure gradient, which is written as a sum of the imposed pressure $(dp_0/dz)\mathbf{k}$, where $\mathbf{k}$ is a unit vector in the vertical direction, and a perturbation pressure gradient $\nabla p'$. The momentum equations are supplemented by the incompressibility conditions $\nabla\cdot\mathbf{u}=0$, which leads to a non-separable elliptic equation for the pressure. The equations are solved on a regular structured grid, using a front-tracking/finite-volume method where the interface between the different fluids is tracked by connected marker points that are advected with the flow and connected by triangular elements. Once the marker points have been advected, a marker function is constructed from the new interface location. The points are also used to compute surface tension, which is then smoothed onto the fluid grid and added to the discrete Navier–Stokes equations. As the marker points are moved and the interface deforms, points are dynamically added or deleted to maintain the point density needed to fully resolve the interface. Since we are interested in the evolution of systems with a constant number of bubbles of a given size, here we do not allow the bubbles to coalesce. Time integration is done by a second order predictor-corrector method, the viscous terms are discretized by second-order centered differences and the advection terms are approximated using a QUICK scheme. The pressure equation is solved using the semi-coarsening multigrid method PFMG / SMG from the HYPRE library(Falgout et al., 2006). The method was introduced by Unverdi and Tryggvason (1992) and for descriptions of the original method, as well as various improvements and refinements, see Tryggvason et al. (2001) and Tryggvason et al. (2011). The method has been used to simulate a large range of multiphase flows, including bubbly flows, see, Yu et al. (1995), Esmaeeli and Tryggvason (1998), Bunner and Tryggvason (1999), Nas and Tryggvason (2003) and Lu et al. (2006), for example. Other implementation of similar ideas and applications to bubbly flows include Dijkhuizen et al. (2010a),Dijkhuizen et al. (2010b),van Sint Annaland et al. (2006), Hao and Prosperetti (2004); Hua and Lou (2007) and Muradoglu and Kayaalp (2006).

Here we assume an insoluble surfactant and no surface diffusion. Since we represent the surface of bubbles by connected marker points that move with the fluid, tracking the surfactant concentration is relatively simple. The total amount of surfactant on a surface element is conserved and the concentration, Γ, simply changes as the area changes, according to $\Gamma Area=\Gamma_o Area_o$, where the subscript o denotes the value at the initial time. The only complication occurs when points are added or deleted and elements

Table 1
The governing parameters.

Parameter	Small	Large
Bubble diameter	0.3	0.36
Void fraction	3.44%	5.94%
Liquid/Bubble density	1.0/0.05	
Liquid/Bubble viscosity	$3.33 \times 10^{-4}/3.33 \times 10^{-5}$	
Surface tension	0.01	0.012
Pressure gradient	0.0018	
Gravitational acceleration	0.05	
Eötvös Number ($Eo = \rho_l g d_0^2/\sigma$)	0.45	0.54
Morton Number ($M = g\mu_l^4/\rho_l\sigma^3$)	6.17×10^{-10}	3.57×10^{-10}

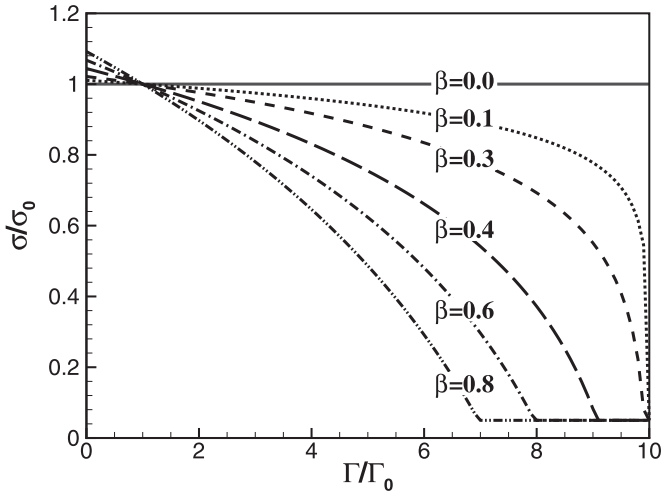

Fig. 1. The non-linear relationship between the surface tension and the surfactant concentration for the results presented here. The relationship is shown for several values of β.

are split or merged. In that case we use a strategy similar to the one discussed in Muradoglu and Tryggvason (2014). Generally we also find that a slight smoothing, using the method described by Taubin (1995), produces a better behaved solution. The surface tension is a function of the surfactant concentration and determined by the Langmuir equation of state (Pawar and Stebe, 1996),

$$\sigma = \sigma_s\big(1 + \beta \ln(1 - \Gamma/\Gamma_\infty)\big). \tag{2}$$

Here, σ_s is the surface tension of a clean interface, Γ_∞ is the maximum interfacial surfactant concentration, and $\beta = RT\Gamma_\infty/\sigma_s$ is the elasticity number which determines the sensitivity of the interfacial tension to variations in the surfactant concentration. R and T are the ideal gas constant and the absolute temperature, respectively.

If we pick a surfactant concentration Γ_o as a reference, then its corresponding surface tension is σ_o, that is,

$$\sigma_o = \sigma_s\big(1 + \beta \ln(1 - \Gamma_o/\Gamma_\infty)\big). \tag{3}$$

and divide equation (2) by equation (3), then we get

$$\frac{\sigma}{\sigma_o} = \frac{1 + \beta \ln(1 - x\Gamma/\Gamma_0)}{1 + \beta \ln(1 - x)}, \tag{4}$$

where $x = \Gamma_o/\Gamma_\infty$ is the dimensionless surfactant coverage. Here we set $x = 0.1$ so the surfactant coverage is far enough from the maximum value. To prevent negative surface tension we follow Muradoglu and Tryggvason (2008) and set the minimum value of $\sigma/\sigma_o = 0.05$. σ/σ_0 is plotted versus Γ/Γ_0 in Fig. 1 for several values of β.

A surfactant has two effects on the surface tension. First of all, adding a surfactant generally reduces the surface tension. We have examined the effect of surface tension, keeping everything else the same, in earlier publications. See, for example, Lu and Tryggvason (2008), Dabiri et al. (2013), and Lu and Tryggvason (2013), and shown that for channel flow the change in lift as the bubbles become more deformable can dramatically influence the structure of the flow. The second effect of a surfactant is to add elasticity to the interface, where the surface tension depends on how much the surface area has changed. In the present study we focus on the effect of the elasticity alone. Thus, we set the initial surfactant concentration and change β. Setting the slope (β) to zero decouples the surface tension from the surfactant concentration. We will refer to this as the clean bubble case, but remind the reader that we are not including the overall reduction in surface tension that generally results from adding surfactants.

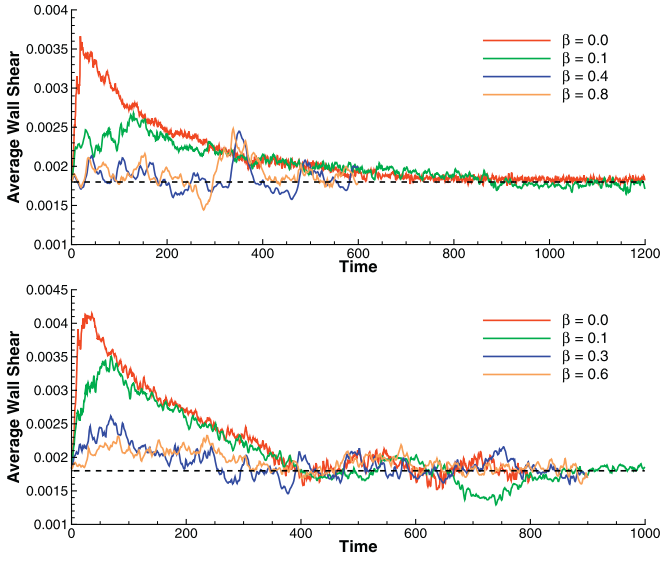

Fig. 2. The wall shear for the small (top) and the large (bottom) bubbles versus time, for four values of β.

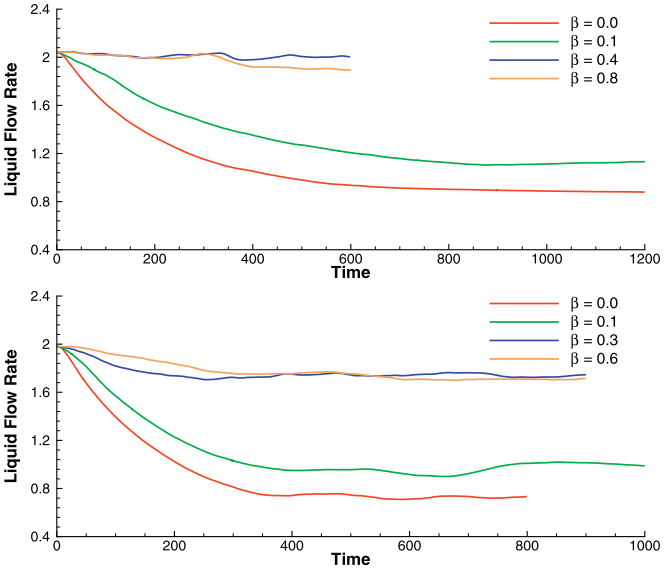

Fig. 3. The liquid flow rate for the small (top) and the large (bottom) bubbles versus time, for four values of β.

3. Results

The effects of surfactants on the flow of many bubbles in a vertical channel flow are examined by placing 24 bubbles in a vertical

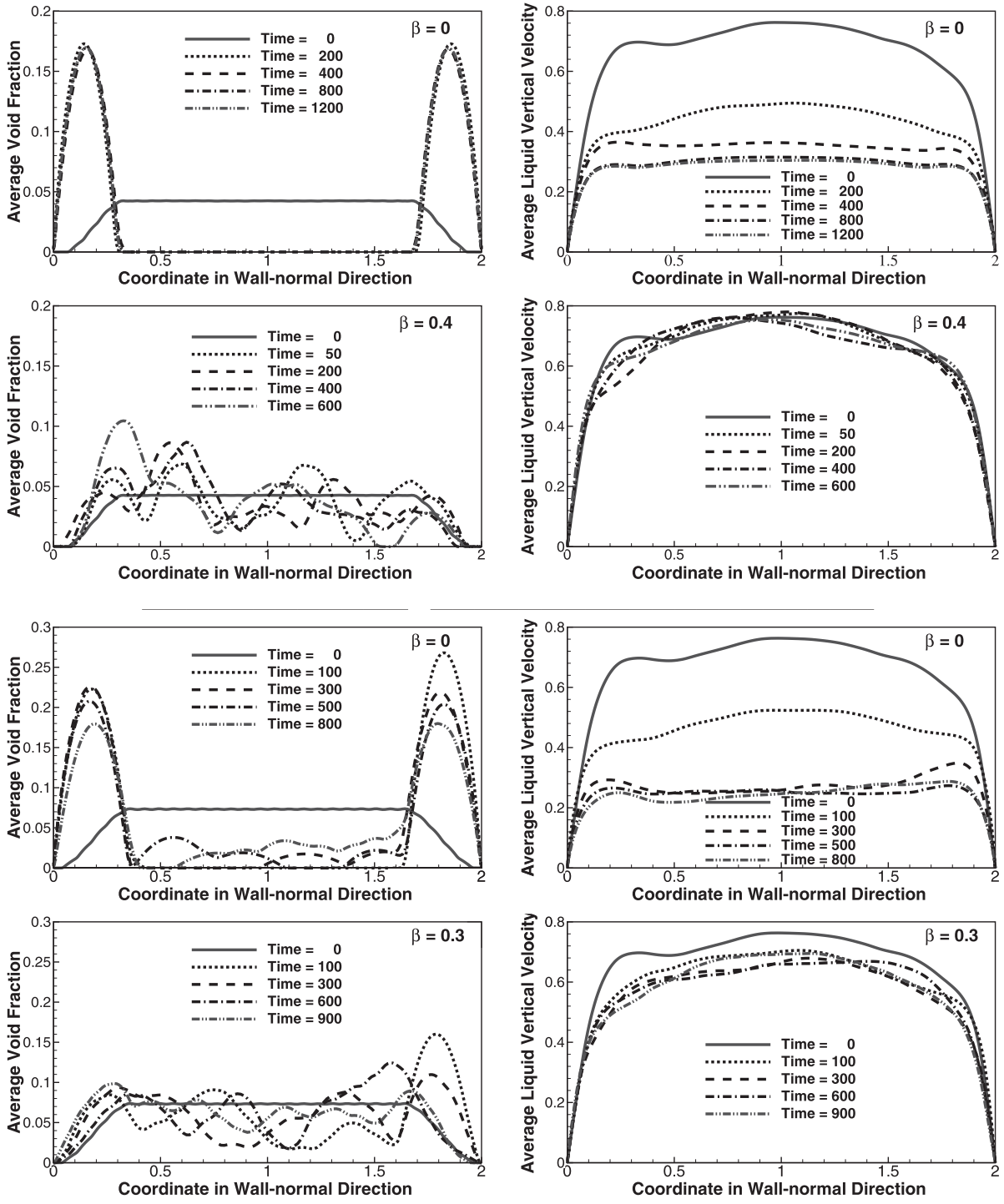

Fig. 4. The void fraction (left column) and the average velocity (right column) versus the wall normal coordinate at several times for both the small (top two rows) and large (bottom two rows) bubbles. Results are shown for clean bubbles in the top (small bubbles) and the third row (large bubbles), in the second row for the small bubbles with surfactants ($\beta = 0.4$), and in the bottom row for the large ones ($\beta = 0.3$).

channel of dimensions $\pi \times 2 \times \pi/2$, resolved by a 256 by 192 by 128 grid in the streamwise, spanwise and wall-normal direction. The grid lines are evenly spaced in the streamwise and spanwise direction, but in the wall-normal direction we use a stretched grid with a grid spacing of 0.004 at the wall, gradually increasing to 0.0157 in the middle of the channel. The initial flow is turbulent, at statistically steady state, with a shear Reynolds number of $Re^+ = u^+h/\nu_l = 127.3$. Here, the friction velocity is $u^+ = \sqrt{\tau_w/\rho_l}$, where ρ_l and ν_l are the density and kinematic viscosity of the liquid respectively, h is the half width of the channel, and $\tau_w = -\beta_o h$ is the wall shear at steady state. Before the bubbles are added, this results in a channel Reynolds number, based on the average velocity and full channel width of about $Re_b \approx 3786$ (Lu and Tryggvason, 2006). Although this is a low value, earlier simulations (Lu and Tryggvason, 2013) have shown that the results are similar to higher shear Reynolds numbers and the low value allows us to use a modest resolution and thus get results faster. Similarly, the number of bubbles included here is relatively modest, compared

to what we have used in other studies (Lu and Tryggvason, 2013; Tryggvason et al., 2016) and what was used by Santarelli and Fröhlich (2015); 2016). We do, however, believe that the present setup is sufficient to answer the question that we are after, namely how does the presence of surfactance affect the flow structure seen in simulations of nearly spherical clean bubbles. Simulations with a modest number of bubbles show the formation of wall layers, the reduction of the Reynolds stresses in the middle of the channel, and the decrease in flow rate just as those with a larger number of bubbles do. We do need a large number of bubbles to see clearly the formation of clusters and voids in the wall layer, but this is a secondary effect, not critical to the question we are addressing. For nearly spherical bubbles where the flow slows down significantly after the formation of the wall-layers, the approach to steady state is very slow so the computer times are an important issue. The bubbles are distributed relatively randomly throughout the domain. The pressure gradient forcing the flow is also modified to account for the reduced average density of the mixture, after the bubbles are added, to keep the shear the same. After a short transient the flow adjusts to the presence of the bubbles, but in general the flow field is not at a statistically steady state and we follow the evolution until a new steady state is reached. For nearly spherical bubbles we did two sets of simulations. The initial flow field, the number of bubbles and their initial locations are the same in all the simulations but the main difference between the two sets is the bubble diameters. We will refer to these as the large and small bubble sets. The values of the governing parameters, which vary slightly between the different sets of runs are listed, in "computational" units, in Table 1. For each set we have performed simulations for four different elasticity numbers, including $\beta = 0$. In each set of simulations the total surfactant on each bubble is the same.

If the average acceleration is zero, then the pressure drop and the weight of the mixture are balanced by the shear force at the wall, both in single phase and multiphase flows, and the wall shear thus provides a convenient quantity to monitor how far the flow is from being at a statistically steady state. In Fig. 2, the wall-shear is plotted versus time for both sets of runs, in both cases for four βs. The evolution is similar in both cases. For $\beta = 0$ there is a rapid rise in the wall shear, followed by a gradual decline that eventually drops it back to the steady state value. As β is increased the initial rise decreases and for the largest β there is very little initial increase, particularly for the larger bubbles (bottom frame). The wall-shear gives us a measure of how far the flow is from equilibrium but not how much it changes with β. Fig. 3 shows the flow rate of the liquid versus time for both sets of runs and four βs for each set. Here it is clear that changing β has a significant effect. For both the small and the large bubbles the flow rate drops significantly when the surface tension remains constant ($\beta = 0$). As β increases, the drop in the flow rate decreases and for the largest two values of β the flow rate hardly changes at all, particularly for the small bubbles (top frame). It is therefore clear that while "clean" bubbles ($\beta = 0$) change the flow rate significantly, non-zero values lead to smaller changes and once β is high enough the flow rate does not change further and there is no dependency on β.

The reason for the differences between the clean bubbles and bubbles with large β, where the surface tension changes significantly, is shown in Fig. 4 where the void fraction and the average liquid velocity are plotted versus the wall-normal coordinate at several different times. The results are shown in the top four frames for the small bubbles and in the bottom four frames for the large bubbles. The void fraction is shown in the left column and the velocity in the right one. The top row shows the results for the clean bubbles ($\beta = 0$) and the second row shows the results for $\beta = 0.4$. Similarly, the third row shows results for the clean large bubbles ($\beta = 0$) and the bottom row for $\beta = 0.3$. For the clean bubbles the void fraction near the walls increases rapidly and at

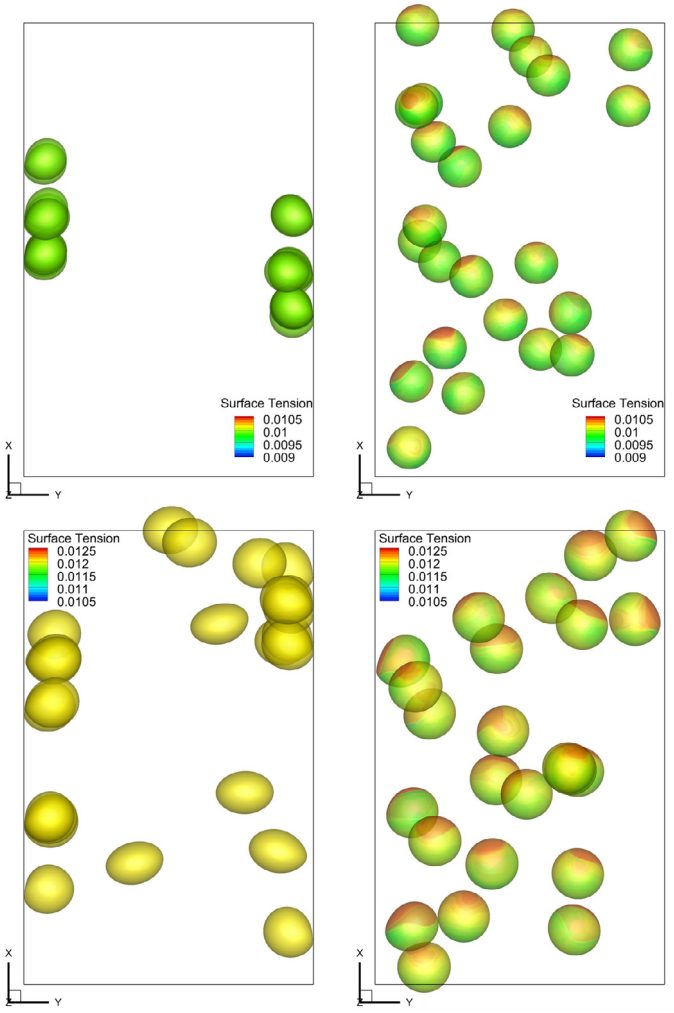

Fig. 5. The bubbles and the surface tension at late times when the flow has reached an approximately steady state. The small bubbles are in the top row and the large ones in the bottom row. The clean bubbles are on the left and the ones with non-zero β on the right. For the bubbles with surfactants we show results for $\beta = 0.4$ for the small bubbles and $\beta = 0.3$ for the large ones.

the last time all the bubbles are collected near the walls, causing a significant reduction in the average velocity as seen in the right frame. When surfactant is present we see a small increase in the void fraction near the walls, but much less than that for the clean bubble cases. For the clean bubble cases the velocity is greatly reduced as the bubbles form wall-layers, but the addition of bubbles with surfactants to a turbulent flow has a much smaller effect and the velocity profile remains for the most part unchanged. As in Fig. 3, the results for the different βs are similar.

Fig. 5 shows the bubble distribution at one time after the flow has reached an approximate statistically steady state. The small bubbles are shown at the top and the large ones at the bottom. The left frames show clean bubbles ($\beta = 0$) and the right column shows bubbles when surfactant is present. For the small bubbles $\beta = 0.4$, and for the large bubbles $\beta = 0.3$. It is immediately clear that the evolution is very different. In the frames on the left the clean bubbles have formed very distinct wall-layers and although some of the larger bubbles remain in the core, the wall-layers are still a dominant feature of the flow. When the surfactant is present the bubbles do not form wall-layers and remain spread out across the channel. This has a profound effect on the flow, as seen in Figs. 2 and 3. In addition to the bubbles themselves, the local surface tension is shows by the coloring of their surface. For the bub-

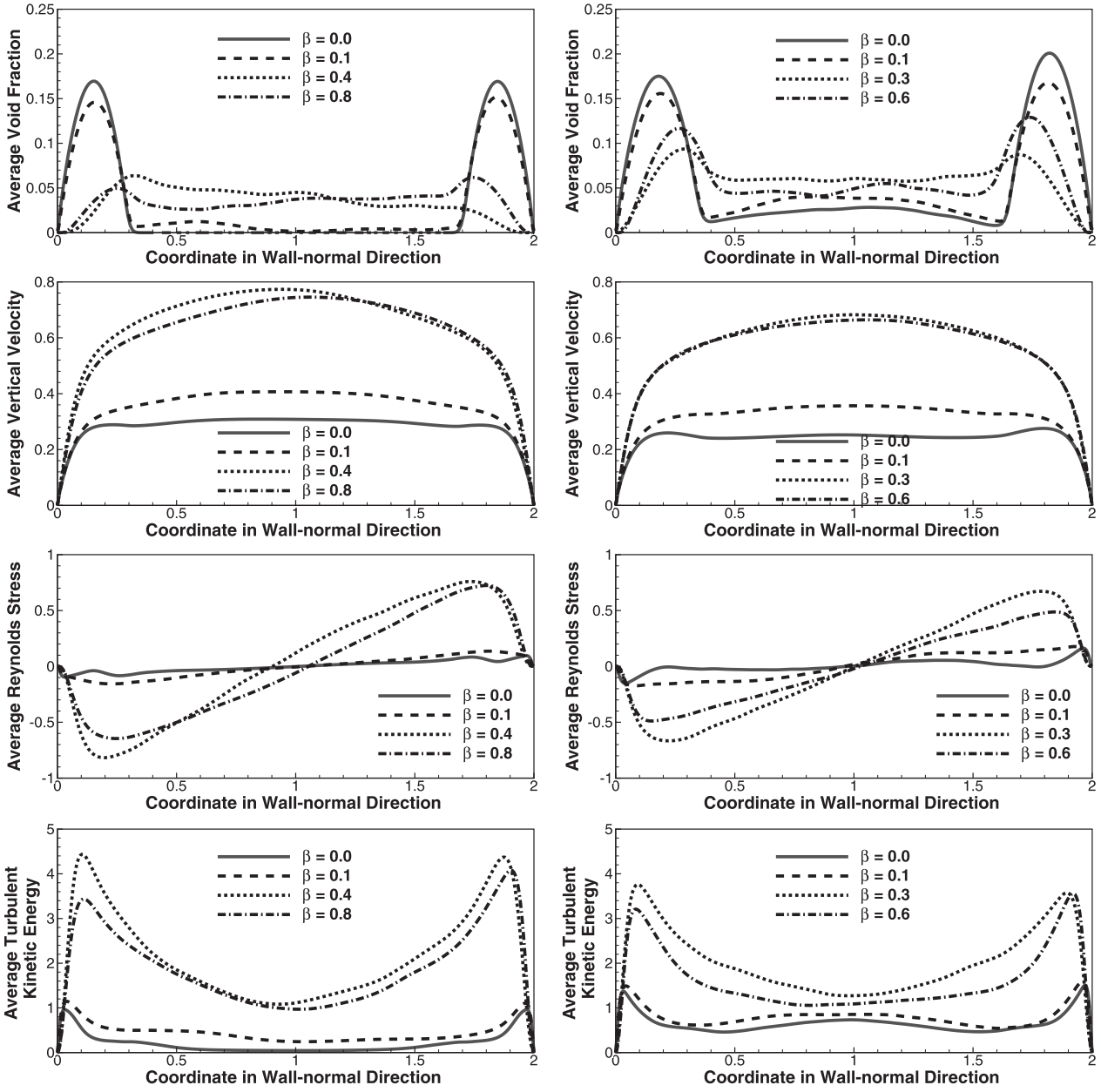

Fig. 6. The steady state results for several averaged quantities in the liquid versus the wall-normal coordinate, after the flow reaches an approximate steady state. The left column shows results for the small bubbles and the results for the large bubbles are shown on the right. (a) The void fraction; (b) The average liquid velocity; (c) The Reynolds stresses $< u'v' >$; (d) The turbulent kinetic energy. The Reynolds stresses and the turbulent kinetic energy are normalized by the friction velocity squared, $(u^+)^2$.

bles with surfactant the surface tension is generally largest at the top and lowest in the back, as expected.

To examine how the structure of the flow changes with the strength of the surfactant we plot, in Fig. 6, a few average quantities versus the wall normal coordinate, obtained by averaging over at least the last 200 time units after the flow reaches an approximate statistically steady state. The left column has results for the small bubbles and the right column for the large bubbles. The void fraction is shown in the top row, the average liquid velocity in the second row, one component of the Reynolds stresses ($< u'v' >$) in the third row, and the turbulent kinetic energy in the bottom row. Notice that we have not averaged over the left and right hand side of the domain so the results are slightly asymmetric due to the finite averaging time. The results reinforce what we have seen for the wall shear and the flow rate. The results for the clean bubbles ($\beta = 0$) are very different than for the two cases with the highest beta ($\beta = 0.4$ and 0.8 for the small bubbles and $\beta = 0.3$ and 0.6 for the large bubbles), with the results for $\beta = 0.1$ in between but closer to the clean bubbles. For the void fraction, which controls the flow, the clean bubbles form a very distinct wall layer, containing all the small bubbles and most of the large bubbles. The wall layer is essentially fully absent for the smaller bubbles with the highest beta but for the larger bubbles void fraction peaks in the wall layers are still visible but are less pronounced and further away from the walls than the peaks for the clean bubbles. The difference in the average liquid velocity is particularly significant. The velocities for the two highest betas are nearly the same for both the large and the small bubbles and much larger than those for the clean bubbles. Indeed, for the highest betas the velocity is comparable to what it would be for single-phase turbulent flow with the same pressure gradient (adjusted to account for the reduced weight of the two fluid mixture). The $< u'v' >$

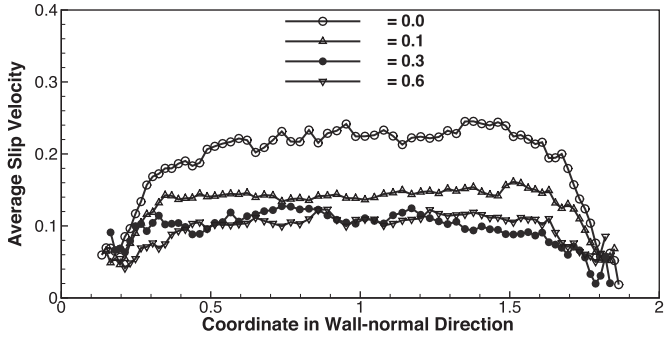

Fig. 7. The effect of β on the slip velocity between the gas and the liquid at steady state, for the large bubbles.

component of the Reynolds stresses (which appear in the average stress balance across the channel) is nearly zero in the bulk of the channel for the clean bubbles, but follow more or less the linear shape usually seen in homogeneous turbulent flow for the highest beta. This shows that while the imposed pressure gradient is balanced by the weight of the mixture in the center of the channel for clean bubbles, this is not the case for the bubbles with sufficiently strong surfactant. For the large bubbles we notice that the Reynolds stresses for the higher beta actually fall below the results for $\beta = 0.3$. The turbulent kinetic energy similarly shows major differences between the clean and nearly clean case and the cases of two largest βs for both the small and the larger bubbles. The significant increase is presumably due to much larger vorticity generation caused by rigidification of interface in cases with surfactants.

The addition of nearly spherical clean bubbles to single phase flow results in a significant reduction in the liquid flow rate as the bubbles are pushed to the walls. The addition of a surfactant eliminates the wall-layers and the reduction in flow rate. The surfactant does, however, reduce the relative velocity of the bubbles compared to the liquid, or the slip velocity. In Fig. 7 we plot the slip velocity versus the wall-normal coordinate for the large bubbles at the statistically steady state. The slip velocity is found by computing the centroid velocity of each bubble and subtracting from it the average velocity of the liquid in each grid-plane parallel to the wall. Thus, there are no data points closer to the wall than about a bubble radius. If the number of bubbles in a particular region is small, this results in noisy data and for the small bubbles there is no data for the bulk, since there are no bubbles there. Thus we only show results for the large bubbles. The results in the bulk show that the slip velocity for the clean bubbles is highest and that there is little difference between the slip velocity for the highest beta.

Another way of looking at how the strength of the surfactant changes the structure of the flow is shown in Fig. 8 where we show a few quantities characterizing the steady state, averaged over the whole channel, versus β, for both series of runs. All quantities are obtained by averaging over at least the last 200 time units, after the flows have reached an approximate steady state. In frame (a) we show the total liquid flow rate. This is the same quantity as shown in Fig. 6, but averaged over the whole channel. Clearly there is a big difference between $\beta = 0$ and the two highest βs, but once β is high enough, doubling it has essentially no impact. Frame (b) shows the total gas flow rate and the results are similar as for the liquid in that there is a big difference between

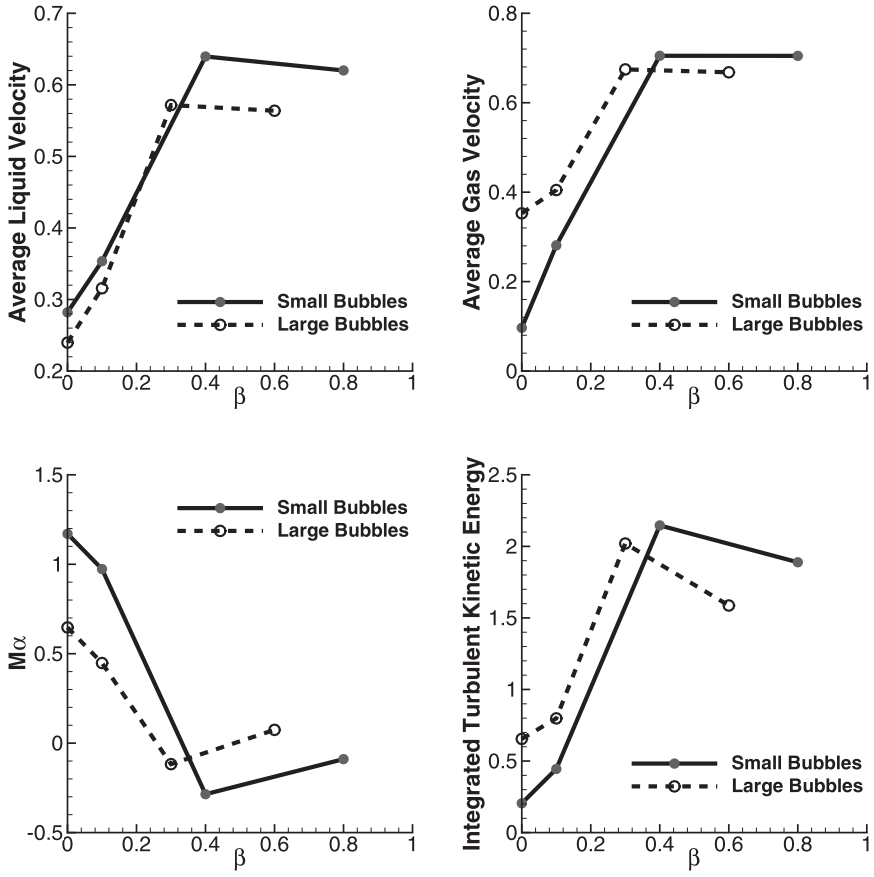

Fig. 8. The effect of β on several averaged values at statistically steady states. (a) Liquid flow rate; (b) The gas flow rate; (c) The void fraction distribution; (d) The integrated turbulent kinetic energy.

$\beta = 0$ and the rest of the results and no change once β is high enough. As Fig. 7 showed, the slip velocity decreases as the surfactant is added, but this figure shows that the higher liquid velocity overcomes this reduction so the total gas flux increases. In frame (c) we examine how the void fraction distribution depends on β by quantifying its shape by the second moment of the void fraction around the channel centerline:

$$M_\alpha = \frac{12}{\alpha_o W^3} \int_0^W \alpha(x)(x - W/2)^2 dx - 1. \quad (5)$$

Here W is the width of the channel, α_o is the average void fraction and we have subtracted the value of the integral for a uniform void fraction to give an M_α with negative values for void fraction peaked near the center of the domain, zero for a uniform distribution, and a positive value for wall peaked distribution. We have also scaled the integral by the value for the uniform distribution to force M to lie in the range $-1 < M_\alpha < 1$. Again, we see a big effect of non-zero β for both sets of runs and little effect once β is high enough. The M_α value for the $\beta = 0$ bubbles clearly shows that the void fraction is non-uniform and most of it is near the wall, while for the highest two βs it is nearly uniform or perhaps slightly peaked in the middle of the channel. In frame (d) we show the total turbulent kinetic energy in a similar way and observe the same behavior as for the other quantities. The increase in the kinetic energy is both due to increased generation of vorticity from the bubble surface once it is immobilized, as well as the absence of bubbles near the wall that disturb and dissipate the wall vortices.

4. Conclusions

The main result from this study is that the addition of surfactants can have a very dramatic influence on the flow rate and the overall flow structure of turbulent bubbly upflows in a vertical channels. The results agree with the experimental studies of So et al. (2002) and Ogasawara et al. (2009), showing that the addition of a surfactant leads to a major change in the void fraction distribution. The bubble clusters seen near walls by (Ogasawara et al., 2009; So et al., 2002) for their weakest surfactant concentration are rarely seen experimentally. However, these structures are seen in computational results for clean bubbles. In experiments, it seems therefore that small clean bubbles are rarely present, presumably both because of natural surfactants usually present and because small clean bubbles are likely to coalesce. Thus, we conclude that experimental data without characterization of the surfactant are likely to be incomplete if small bubbles are present, and thus difficult to compare with theoretical and computational models.

Acknowledgement

This work is supported by the Consortium for Advanced Simulation of Light Water Reactors (CASL), an Energy Innovation Hub for Modeling and Simulations of Nuclear Reactors under U.S. Department of Energy (grant number DE-AC05-00OR22725).

References

Balcázar, N., Lehmkuhl, O., Rigola, J., Oliva, A., 2015. A multiple marker level-set method for simulation of deformable fluid particles. Int. J. Multiphase Flow 74, 125–142.
Bois, G., du Cluzeau, A., 2017. FEDSM2017-69128: DNS of turbulent bubbly flows in plane channels using the front tracking algorithm of TRIOCFD. In: Proceedings of the ASME FEDSM'00 ASME 2017 Fluids Engineering Division Summer Meeting July 30-August 3, 2017, Waikoloa, Hawaii.
Bolotnov, I.A., 2013. Influence of bubbles on the turbulence anisotropy. J. Fluids Eng. 135. 051301 (9 pages).
Bolotnov, I.A., Jansen, K.E., Drew, D.A., Oberai, A.A., Lahey, R.T., Podowski, M.Z., 2011. Detached direct numerical simulations of turbulent two-phase bubbly channel flow. Int. J. Multiphase Flow 37, 647–659.
Bolotnov, I.A., Lahey, R.T., Drew, D.A., Jansen, K.E., 2008. Turbulent cascade modeling of single and bubbly two-phase turbulent flows. Int. J. Multiphase Flow 34, 1142–1151.
Bunner, B., Tryggvason, G., 1999. Direct numerical simulations of three-dimensional bubbly flows. Phys. Fluids 11, 1967–1969.
Bunner, B., Tryggvason, G., 2003. Effect of bubble deformation on the stability and properties of bubbly flows. J. Fluid Mech. 495, 77–118.
Clift, R., Grace, J., Weber, M., 1978. Bubbles, drops, and particles. Academic Press.
Dabiri, S., Lu, J., Tryggvason, G., 2013. Transition between regimes of a vertical channel bubbly upflow due to bubble deformability. Phys. Fluids 25. 102110 (12 pages).
Dijkhuizen, W., Roghair, I., Annaland, M.V.S., Kuipers, J., 2010. DNS of gas bubbles behaviour using an improved 3d front tracking model–drag force on isolated bubbles and comparison with experiments. Chem. Eng. Sci. 65, 1415–1426.
Dijkhuizen, W., Roghair, I., Annaland, M.V.S., Kuipers, J., 2010. DNS of gas bubbles behaviour using an improved 3d front tracking model–model development. Chem. Eng. Sci. 65, 1427–1437.
Esmaeeli, A., Tryggvason, G., 1998. Direct numerical simulations of bubbly flows. part i—low Reynolds number arrays. J. Fluid Mech. 377, 313–345.
Falgout, R.D., Jones, J.E., Yang, U.M., 2006. The design and implementation of hypre, a library of parallel high performance preconditioners. In: Bruaset, A.M., Tveito, A. (Eds.), Numerical Solution of Partial Differential Equations on Parallel Computers, 51. Springer-Verlag, pp. 267–294.
Fukuta, M., Takagi, S., Matsumoto, Y., 2005. The effect of surface velocity on lift force for a spherical bubble in a linear shear flow. Theor. Appl. Mech. Jpn 54, 227–234.
Fukuta, M., Takagi, S., Matsumoto, Y., 2008. Numerical study on the shear-induced lift force acting on a spherical bubble in aqueous surfactant solutions. Phys. Fluids 20, 040704.
Hao, Y., Prosperetti, A., 2004. A numerical method for three-dimensional gas–liquid flow computations. J. Comput. Phys. 196, 126–144.
Hua, J., Lou, J., 2007. Numerical simulation of bubble rising in viscous liquid. J. Comput. Phys. 222, 769–795.
Jan, Y.-J., 1994. Computational Studies of Bubble Dynamics. The University of Michigan.
de Jesus, W.C., Roma, A.M., Pivello, M.R., Villar, M.M., da Silveira-Neto, A., 2015. A 3D front-tracking approach for simulation of a two-phase fluid with insoluble surfactant. J. Comput. Phys. 281, 403–420.
Ling, Y., Fuster, D., Zaleski, S., Tryggvason, G., 2017. Spray formation in a quasi-planar gas-liquid mixing layer at moderate density ratios: a numerical closeup. Phys. Rev. Fluids 014005.
Lu, J., Biswas, S., Tryggvason, G., 2006. A DNS study of laminar bubbly flows in a vertical channel. Int. J. Multiphase Flow 32, 643–660.
Lu, J., Tryggvason, G., 2006. Numerical study of turbulent bubbly downflows in a vertical channel. Phys. Fluids 18. 103302 (10 pages).
Lu, J., Tryggvason, G., 2008. Effect of bubble deformability in turbulent bubbly upflow in a vertical channel. Phys. Fluids 20, 040701.
Lu, J., Tryggvason, G., 2013. Dynamics of nearly spherical bubbles in a turbulent channel upflow. J. Fluid Mech. 732, 166–189.
Muradoglu, M., Kayaalp, A.D., 2006. An auxiliary grid method for computations of multiphase flows in complex geometries. J. Comput. Phys. 214, 858–877.
Muradoglu, M., Tryggvason, G., 2008. A front-tracking method for computation of interfacial flows with soluble surfactants. J. Comput. Phys. 227, 2238–2262.
Muradoglu, M., Tryggvason, G., 2014. Simulations of soluble surfactants in 3d multiphase flow. J. Comput. Phys. 274, 737–757.
Nas, S., Tryggvason, G., 2003. Thermocapillary interaction of two bubbles or drops. Int. J. Multiphase Flow Vol. 29, 1117–1135.
Ogasawara, T., Takagi, S., Matsumoto, Y., 2009. Influence of local void fraction distribution on turbulent structure of upward bubbly flow in vertical channel. In: The 6th International Symposium on Measurement Techniques for Multiphase Flows, Journal of Physics: Conference Series, 147. 012027 (10 pages).
Pawar, Y., Stebe, K., 1996. Marangoni effects on drop deformation in an extensional flow: the role of surfactant physical chemistry. i. insoluble surfactants. Phys. Fluids 8, 1738–1751.
Santarelli, C., Fröhlich, J., 2015. Direct numerical simulations of spherical bubbles in vertical turbulent channel flow. Int. J. Multiphase Flow 75, 174–193.
Santarelli, C., Fröhlich, J., 2016. Direct numerical simulations of spherical bubbles in vertical turbulent channel flow. influence of bubble size and bidispersity. Int. J. Multiphase Flow 81, 27–45.
Serizawa, A., Kataoka, I., Michiyoshi, I., 1975. Turbulence structure of air-water bubbly flow–II. local properties. Int. J. Multiphase Flow 2, 235–246.
van Sint Annaland, M., Dijkhuizen, W., Deen, N., Kuipers, J., 2006. Numerical simulation of gas bubbles behaviour using a 3d front tracking method. AIChE J. 52, 99–110.
So, S., Morikita, H., Takagi, S., Matsumoto, Y., 2002. Laser doppler velocimetry measurement of turbulent bubbly channel flow. Exp. Fluids 33, 135–142.
Takagi, S., Matsumoto, Y., 2011. Surfactant effects on bubble motion and bubbly flows. Ann. Rev. Fluid Mech. 43, 615–636.
Takagi, S., Ogasawara, T., Matsumoto, Y., 2008. The effects of surfactant on the multiscale structure of bubbly flows. Philos. Trans. R. Soc. A: 366, 2117–2129.

Tanaka, M., 2011. Computational simulations and applications. In: Zhu, J. (Ed.), Numerical study on flow structures and heat transfer characteristics of turbulent bubbly upflow in a vertical channel. InTech, Rijeka, Croatia, pp. 119–142.

Taubin, G., 1995. A signal processing approach to fair surface design. In: Proceedings of the 22Nd Annual Conference on Computer Graphics and Interactive Techniques. ACM, New York, NY, USA, pp. 351–358. doi:10.1145/218380.218473.

Tryggvason, G., Bunner, B., Esmaeeli, A., Juric, D., Al-Rawhai, N., Tauber, W., Han, J., Nas, S., Jan, Y.-J., 2001. A front tracking method for the computations of multiphase flow. J. Comput. Phys. 169, 708–759.

Tryggvason, G., Ma, M., Lu, J., 2016. DNS assisted modeling of bubbly flows in vertical channels. Nucl. Sci. Eng. 184, 312–320.

Tryggvason, G., Scardovelli, R., Zaleski, S., 2011. Direct numerical simulations of gas-liquid multiphase flows. Cambridge University Press.

Unverdi, S.O., Tryggvason, G., 1992. A front-tracking method for viscous, incompressible, multi-fluid flows. J. Comput. Phys. 100, 25–37.

Yu, P.-W., Ceccio, S., Tryggvason, G., 1995. The collapse of a cavitation bubble in shear flows-a numerical study. Phys. Fluids 7, 2608–2616.